ISSN 1674-1056
http://cpb.iphy.ac.cn
http://iopscience.iop.org/cpb
中国物理 B
Chinese Physics
中国物理 Chinese Physics B

SnS_2 quantum dots: Facile synthesis, properties, and applications in ultraviolet photodetector

Yao Li(李尧), Libin Tang (唐利斌), Rujie Li(李汝劼), Jinzhong Xiang(项金钟), Kar Seng Teng, Shu Ping Lau(刘树平)

Citation: Chin. Phys. B . 2019, 28(3): 037801. **doi:** 10.1088/1674-1056/28/3/037801
Journal homepage: http://cpb.iphy.ac.cn; http://iopscience.iop.org/cpb

What follows is a list of articles you may be interested in

Magneto-optical properties of self-assembled InAs quantum dots for quantum information processing

Jing Tang(唐静), Xiu-Lai Xu(许秀来)
Chin. Phys. B . 2018, 27(2): 027804. **doi:** 10.1088/1674-1056/27/2/027804

Temperature-dependent photoluminescence of size-tunable ZnAgInSe quaternary quantum dots

Qi Ding(丁琪), Xiao-Song Zhang(张晓松), Lan Li(李岚), Jian-Ping Xu(徐建萍), Ping Zhou(周平), Xiao-Fei Dong(董晓菲), Ming Yan(晏明)
Chin. Phys. B . 2017, 26(6): 067804. **doi:** 10.1088/1674-1056/26/6/067804

Temperature dependence of the photoluminescence of MnS/ZnS core–shell quantum dots

Fang Dai-Feng, Ding Xing, Dai Ru-Cheng, Zhao Zhi, Wang Zhong-Ping, Zhang Zeng-Ming
Chin. Phys. B . 2014, 23(12): 127804. **doi:** 10.1088/1674-1056/23/12/127804

Optimization of InAs/GaAs quantum-dot structures and application to 1.3-μm mode-locked laser diodes

Li Mi-Feng, Ni Hai-Qiao, Ding Ying, Bajek David, Kong Liang, Cataluna Maria Ana, Niu Zhi-Chuan
Chin. Phys. B . 2014, 23(2): 027803. **doi:** 10.1088/1674-1056/23/2/027803

Investigation of ultrafast dynamics of CdTe quantum dots by femtosecond fluorescence up-conversion spectroscopy

Yao Guan-Xin, L¨u Liang-Hong, Gui Mei-Fang, Zhang Xian-Yi, Zheng Xian-Feng, Ji Xue-Han, Zhang Hong, Cui Zhi-Feng
Chin. Phys. B . 2012, 21(10): 107801. **doi:** 10.1088/1674-1056/21/10/107801

SPECIAL TOPIC — Photodetector: Materials, physics, and applications

SnS_2 quantum dots: Facile synthesis, properties, and applications in ultraviolet photodetector*

Yao Li(李尧)[1], Libin Tang (唐利斌)[1,2,†], Rujie Li(李汝劼)[2,3], Jinzhong Xiang(项金钟)[1,‡], Kar Seng Teng[4], and Shu Ping Lau(刘树平)[5]

[1] School of Materials Science and Engineering, Yunnan University, Kunming 650091, China
[2] Kunming Institute of Physics, Kunming 650223, China
[3] School of Physics, Beijing Institute of Technology, Beijing 100081, China
[4] College of Engineering, Swansea University, Bay Campus, Fabian Way, Swansea SA1 8EN, United Kingdom
[5] Department of Applied Physics, The Hong Kong Polytechnic University, Hong Kong, China

(Received 7 October 2018; revised manuscript received 7 January 2019; published online 18 January 2019)

Tin sulfide quantum dots (SnS_2 QDs) are n-type wide band gap semiconductor. They exhibit a high optical absorption coefficient and strong photoconductive property in the ultraviolet and visible regions. Therefore, they have been found to have many potential applications, such as gas sensors, resistors, photodetectors, photocatalysts, and solar cells. However, the existing preparation methods for SnS_2 QDs are complicated and require a high temperature and high pressure environments; hence they are unsuitable for large-scale industrial production. An effective method for the preparation of monodispersed SnS_2 QDs at normal temperature and pressure will be discussed in this paper. The method is facile, green, and low-cost. In this work, the structure, morphology, optical, electrical, and photoelectric properties of SnS_2 QDs are studied. The synthesized SnS_2 QDs are homogeneous in size and exhibit good photoelectric performance. A photoelectric detector based on the SnS_2 QDs is fabricated and its J–V and C–V characteristics are also studied. The detector responds under $\lambda = 365$ nm light irradiation and reverse bias voltage. Its detectivity approximately stabilizes at 10^{11} Jones at room temperature. These results show the possible use of SnS_2 QDs in photodetectors.

Keywords: SnS_2, quantum dots, photoelectric properties, photodetector

PACS: 78.67.Hc, 84.60.Jt, 85.60.Gz **DOI:** 10.1088/1674-1056/28/3/037801

1. Introduction

In recent years, there has been great interest in two-dimensional (2D) materials due to their high specific surface areas and excellent electronic properties.[1–3] Tin disulfide (SnS_2) is one of the members of IV:VI binary compounds in 2D metal chalcogenides. It is an n-type compound semiconductor with layered and hexagonal CdI_2 structures.[4] This structural unit has a two-layer sandwich structure, which is comprised of hexagonally closely packed S^{2-} with Sn^{4+}. One Sn^{4+} and six S^{2-} form an octahedral coordination, which means that S^{2-} is AB–AB hexagonal close packing and the metal Sn^{4+} is between the double-deck S^{2-}. There is covalent bonding in the inner layer and weak van der Waals force between the layers. The bulk SnS_2 material exhibits non-toxicity and good chemical stability. Furthermore, the material can be produced at relatively low cost as its reactant is readily available. Hence, SnS_2 material has been studied for use in the fields of photoelectric detectors,[5,6] sensors,[7] and lithium ion batteries.[8]

Semiconductor quantum dots (QDs) are quasi-zero-dimensional nanocrystals with electrons and holes confined in all three dimensions.[9,10] Due to the confinement, the movement of the carriers is limited to a certain space, resulting in an increase in electron kinetic energy. This leads to an increase in the material energy gap and the exciton energy, thus producing a quantum size effect where the band width is ultimately determined by the size of the quantum dot. SnS_2 QDs, with size between 1 nm and 10 nm, have been applied in fields of photoelectric detector,[11] solar photocatalyst,[12] and photovoltaic solar cell.[13] These devices have demonstrated good detection capability, high sensitivity, and high energy conversion efficiency.

Low-cost solution-based synthesis of colloidal semiconductor QDs has attracted increasing attention due to their applications in photodetectors.[14] The colloidal preparation methods of SnS_2 QDs include liquid-phase exfoliation (LPE),[15] solution thermal synthesis,[12] hot injection,[13,16] and wet chemistry methods.[17] The QDs prepared by colloidal chemistry are also known as colloidal quantum dots (CQDs). The colloidal chemistry method is a wet chemical method that

*Project supported by the Equipment Pre-research Fund under the Equipment Development Department (EDD) of China's Central Military Commission (CMC) (Grant No. 1422030209), the Innovation Team Program of China North Industries Group Corporation Limited (NORINCO) Group (Grant No. 2017CX024), and the National Natural Science Foundation of China (Grant Nos. 61106098 and 11864044).

†Corresponding author. E-mail: scitang@163.com
‡Corresponding author. E-mail: jzhxiang@ynu.edu.cn

© 2019 Chinese Physical Society and IOP Publishing Ltd

uses organic ligand molecules to wrap the surface of growing QDs to control particle agglomeration.[18] The general method involves rapid introduction of precursor solution into a high-boiling-point organic solvent, which would generate a lot of nucleation centers. The coordination solvent molecules would dynamically adsorb on the surface of the growing small particles to prevent or limit the growth of particles and to control the particle growing time in the Qstwald ripening process (e.g., smaller particles have higher surface free energy; the small sol particles dissolve and redeposit on larger sol particles to achieve the growth of the macroparticles), hence resulting in monodispersed QDs. Small, homogeneous, and high-quality QDs can be synthesized using this method by controlling the growth time. Colloidal QDs can be produced in different forms, such as solution, powder, or film. Furthermore, it is easy to implement QDs surface engineering, and different organic ligand molecules can be used to envelop the surface of QDs to make it hydrophilic/hydrophobic. The preparation method of SnS_2 QDs in this work does not require high temperature and high pressure processes. It involves mild reaction conditions and facile processes to synthesize small and homogeneous SnS_2 QDs that show good dispersion and stability in solvent.

2. Experimental

2.1. Materials

The chemical reagents used in the experiments were purchased and used without further purification.

$SnCl_4{\cdot}5\ H_2O$ (analytical reagent, AR), $Na_2S{\cdot}9H_2O$ (AR 98.0%) and $C_{12}H_{25}NaO_3S$ (AR 98.0%) were purchased from Tianjin Fengchuan Chemical Reagent Co., Ltd. (Tianjin, China). Ethanol (99.8% AR) and ethylene glycol (AR) were purchased from Chengdu Kelong Chemical Co., Ltd. (Sichuan, China).

2.2. Preparation of SnS_2 QDs

The preparation process of the SnS_2 QDs is shown in Fig. 1(a). Below is the chemical equation of this experiment

$$SnCl_4 + 2Na_2S = SnS_2 \downarrow + 4NaCl. \quad (1)$$

0.2 mol·L^{-1} Na_2S solution and 0.2 mol·L^{-1} $SnCl_4$ solution were prepared as the sulfur source and tin source, respectively. The entire preparation process was performed on a heating plate at 50 °C. To obtain 0.002 g SnS_2, 548 μL $SnCl_4$ and 1073 μL Na_2S were introduced respectively to test tubes. Then 0.03 mol·L^{-1} $C_{12}H_{25}NaO_3S$ (as surfactant) were added respectively to Na_2S solution and $SnCl_4$ solution (the volume ratio was 1:1), and the two mixtures were thoroughly mixed. Subsequently, $SnCl_4$ mixed solution was slowly dripped into Na_2S mixed solution under constant stirring for 10 min until the reaction was completed. The products were centrifuged at 3000 rpm for 5 min. After centrifugation, the precipitate was reserved and a mixed solution of deionized water and ethanediol (the volume ratio was 1:1) was added and centrifuged again. This process was repeated twice. Once completed, the resultant yellow colored precipitate at the bottom of the solution was the desired SnS_2 QDs. Finally, ethylene glycol (as dispersant) was added to the yellow precipitate and collected via a pipette to a plastic test tube. The SnS_2 QDs were obtained.

2.3. Characterization techniques

High-resolution transmission electron microscopy (HRTEM) was performed on a JEM-2100 electron microscope operating at 200 kV. The Raman spectrum was obtained at an ambient temperature on a Renishaw inVia Raman microscope with an argon-ion laser with an excitation wavelength of 514.5 nm. The Fourier-transform infrared (FTIR) spectra were measured by a NicoletiS10 infrared spectrometer using the KBr pellet technique. Optical properties were characterized by ultraviolet (UV)–visible (Vis) absorption spectra (SHIMADZU, Uv-1700) and fluorescence (Hitachi F-4500) spectrometers. Functional groups on the surface of the SnS_2 QDs were verified by x-ray photoelectron spectroscopy (XPS) using Al $K\alpha$ radiation PHI VersaProbe II. X-ray diffraction (XRD) of the samples was measured using Rigaku D/Max-23 at room temperature. The surface morphology and roughness of SnS_2 QDs were investigated by scanning electron microscope (SEM) using Hitachi S3400 (Japan) and atomic force microscope (AFM) using SPA-400, respectively. The current density–voltage (J–V) characteristics were measured using Keithley 2400 source meter. The fluorescence effect was analyzed by a camera-obscura ultraviolet analyzer (ZF-7N). The images of the interdigital electrodes were observed using LEICA optical microscope (DM 2700M). The capacitance–voltage (C–V) curve was measured using a semiconductor device analyzer (KEYSIGHT B1500A).

3. Results and discussion

3.1. Characterization of SnS_2 QDs

The SnS_2 QDs are characterized using transmission electron microscopy (TEM), as shown in Fig. 1(b). The QDs are spherical in shape and their sizes are uniformly distributed. The size distribution of the SnS_2 QDs is analyzed as shown in the inset of Fig. 1(b), which follows a Gaussian distribution as indicated by the fitting curve. The average diameter of the SnS_2 QDs is 4.2 nm with full width at half maximum (FWHM) of 0.98 nm, which shows that the size distribution range of the QDs prepared by this method is narrow, hence demonstrating the uniformity of the QDs. Figure 1(c) is a high-resolution TEM image of a typical single SnS_2 QD, which is indicated by a yellow square in Fig. 1(b). The clear and bright lattice fringe demonstrates good crystallinity of the QDs. Fast

Fourier-transform (FFT) has been performed as shown in the inset of Fig. 1(c), which reveals hexagonal crystal structures of the QDs. Figure 1(d) is the line profile of the lattice planes in Fig. 1(c), showing that the inter-planar crystal spacing is 0.277 nm.[19] The morphology of SnS_2 QDs' thin film has been studied using AFM, as shown in Fig. 1(e), and the height analysis of QDs *A*, *B*, and *C* is shown in the inset. They are randomly selected and their height ranges from 4.1 nm to 4.6 nm, which is very close to the average size of the QDs (4.2 nm) obtained from the TEM image. Figure 1(f) shows the XRD pattern of the SnS_2 QDs. The peaks at $2\theta = 28.2°$, 33.1°, 50.6°, and 52.7° correspond to lattice planes (100), (101), (110), and (111).[20] The Si peak is observed in the XRD as the SnS_2 QDs are deposited on a silicon wafer. The Raman spectrum of the SnS_2 QDs is shown in Fig. 1(g). The vibrational modes of the QDs are studied. Two prominent peaks, such as E_g peak ($\sim 220\ cm^{-1}$) and A_{1g} peak ($\sim 317\ cm^{-1}$), are observed. The Raman vibrational mode E_g corresponds to a non-degenerate in-plane vibration mode, whereas A_{1g} corresponds to the Sn–S bonds of vertical out-of-plane vibration.[21] The UV–Vis spectrum of SnS_2 QDs' aqueous solution is shown in Fig. 1(h), which shows an absorption peak at 225 nm in the ultraviolet range. This indicates a blue shift as compared to the absorption peak of 500 nm for SnS_2 bulk material.[22] Such a phenomenon is attributed to the quantum confinement effect. The aqueous solutions of SnS_2 QDs are shown in the inset of Fig. 1(h). On the left is the pale yellow solution of SnS_2 QDs under natural light, and on the right is the SnS_2 QDs solution under 365 nm ultraviolet illumination, which demonstrates the fluorescence effect.

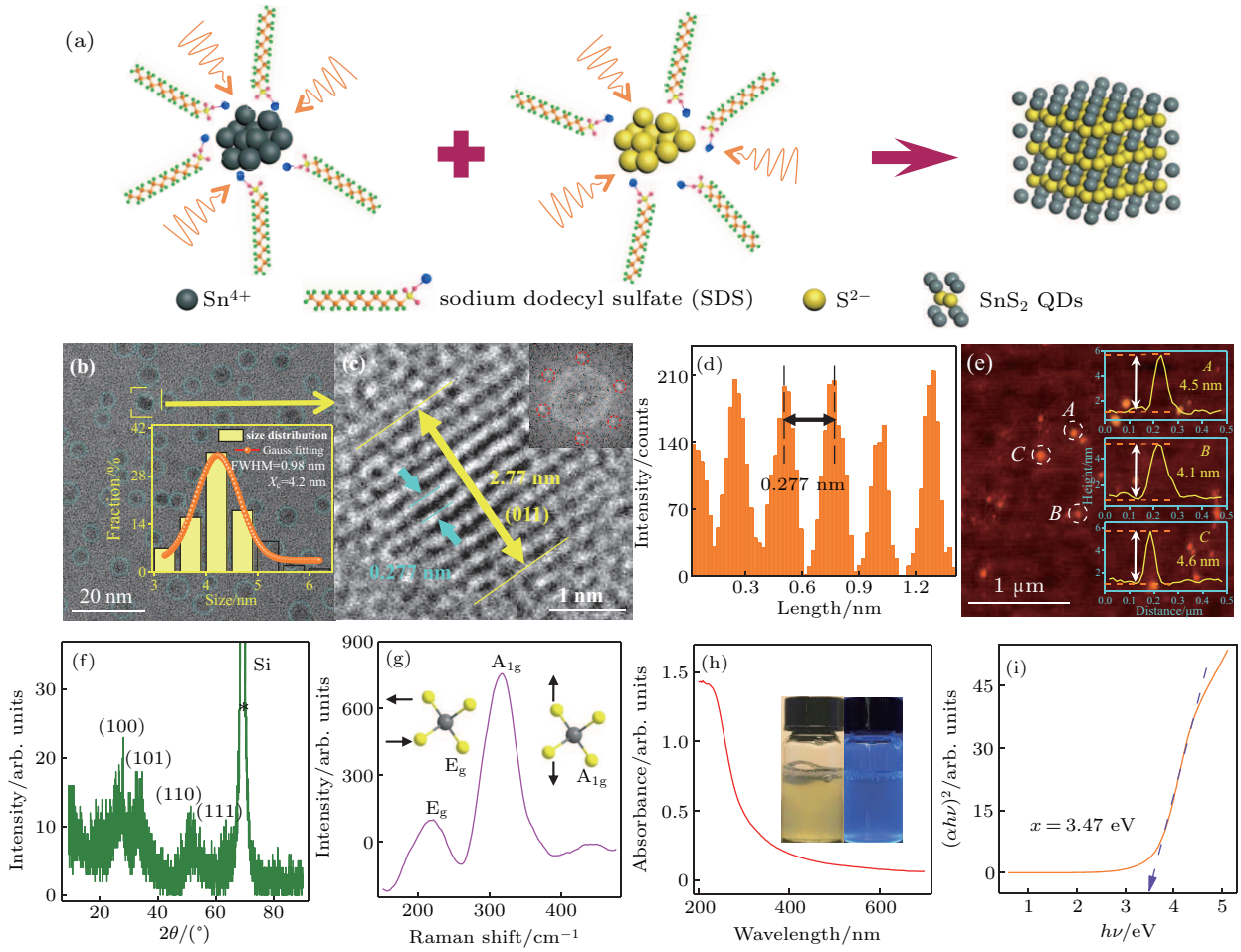


Fig. 1. (a) Schematic representation of the synthesis of SnS_2 QDs. (b) The TEM image of SnS_2 QDs and the size distribution of the SnS_2 QDs. (c) The HRTEM image of the SnS_2 QDs with lattice fringe spacing of 0.277 nm. (d) The line-profile analysis of the SnS_2 QDs as shown in (c). (e) AFM image of the SnS_2 QDs on Si substrate. (f) The XRD pattern of the SnS_2 QDs. (g) The Raman spectrum of the SnS_2 QDs on Si substrate with schematics of E_g and A_{1g} Raman vibrational modes. (h) UV–Vis absorption spectra of SnS_2 QDs aqueous solution. (i) Tauc plot for estimating E_g of SnS_2 QDs.

The bandgap energy E_g of the SnS_2 QDs can be obtained by the Tauc plot using[23]

$$\alpha h\nu = D(h\nu - E_g)^{1/2}, \tag{2}$$

where α is the absorption coefficient, D is a constant, $h\nu$ is the photon energy, and E_g is the bandgap energy. The bandgap energy E_g of SnS_2 QDs is estimated at 3.47 eV from the curve of $(\alpha h\nu)^2$ vs. $h\nu$ in Fig. 1(i). The estimated value is larger than the bulk value of 2.31 eV[24] due to the quantum effect; the larger E_g makes SnS_2 QDs suitable for fabricating solar-blind UV detector. Under the effective-mass approximation,

the size dependence of the bandgap of QDs can be represented as follows:[25]

$$E_g \approx E_{g(0)} + \frac{\hbar^2\pi^2}{2\mu R^2} - \frac{1.8e^2}{\varepsilon R}, \quad (3)$$

where $E_{g(0)}$ is the bandgap of bulk SnS_2 (2.31 eV), $\hbar$ is the reduced Planck constant, μ is the reduced mass of excitation, R is the radius of SnS_2 QDs, e is the electron charge, and ε is the dielectric constant of SnS_2 (20).[15] The calculated E_g value is 3.01 eV, which is close to the fitted value of 3.47 eV.

The photoluminescence (PL) study of the as-prepared SnS_2 QDs solution is carried out using excitation wavelengths ranging from 360 nm to 400 nm. Figure 2(a) shows the PL spectra of the QDs solution excited by various wavelengths. A wide PL peak can be observed at $\lambda = 465$ nm. The normalized PL spectra of the QDs are also shown in the inset of Fig. 2(a). Figure 2(b) shows the photoluminescence excitation (PLE) spectra of the QDs. A PLE peak is situated at $\lambda = 377$ nm with different receiving energies λ_{Em}, which reveals that different λ_{Em} values have no effect on the peak position. The PLE results are in good agreement with the UV absorption results. The normalized PLE spectra of the QDs are shown in the inset of Fig. 2(b). The elemental analysis of the SnS_2 QDs is performed using energy-dispersive x-ray spectroscopy (EDS) as shown in Fig. 2(c). The SEM image is shown in the inset of Fig. 2(c), and what we have observed are aggregates of SnS_2 QDs. The S and Sn peaks indicate the presence of sulphur and tin, respectively. The small C and O peaks reveal the existence of a low-density of carbon and oxygen functional groups, respectively, in the QDs prepared using this method. This could be due to the fact that the surfactant is not removed entirely during the preparation process. The chemical composition of the SnS_2 QDs is analyzed using XPS. The full-scan XPS spectrum is shown in Fig. 2(d). The spectrum shows the Sn $3d_{5/2}$ peak at 486.1 eV, Sn $3d_{3/2}$ peak at 495.5 eV, Sn $3p_{3/2}$ peak at 716.6 eV, Sn $3p_{1/2}$ peak at 758.5 eV, Sn 4d peak at 25.8 eV, O 1s peak at 529.4 eV, and C 1s peak at 285.4 eV. The S 2p peak at 167.7 eV can be observed in the inset of Fig. 2(d). The presence of the C and O peaks could be due to the C and O functional groups induced by the surfactant, respectively, as well as exposure of the SnS_2 QDs to air. As shown in Fig. 2(e), the S 2p core level peak is fitted with three peaks at 164.5 eV, 165.6 eV, and 167.8 eV, corresponding to S $2p_{3/2}$, S $2p_{1/2}$, and S–O respectively.[26] The Sn 3d core level peak is shown in Fig. 2(f); it was deconvoluted into two peaks, namely, Sn $3d_{5/2}$ and Sn $3d_{3/2}$. It can be seen that the area of Sn^{4+}–S^{2-} is larger than the area of Sn^{2+}–S^{2-} in the fitted peaks, which indicates a very small amount of SnS in SnS_2 QDs.[27]

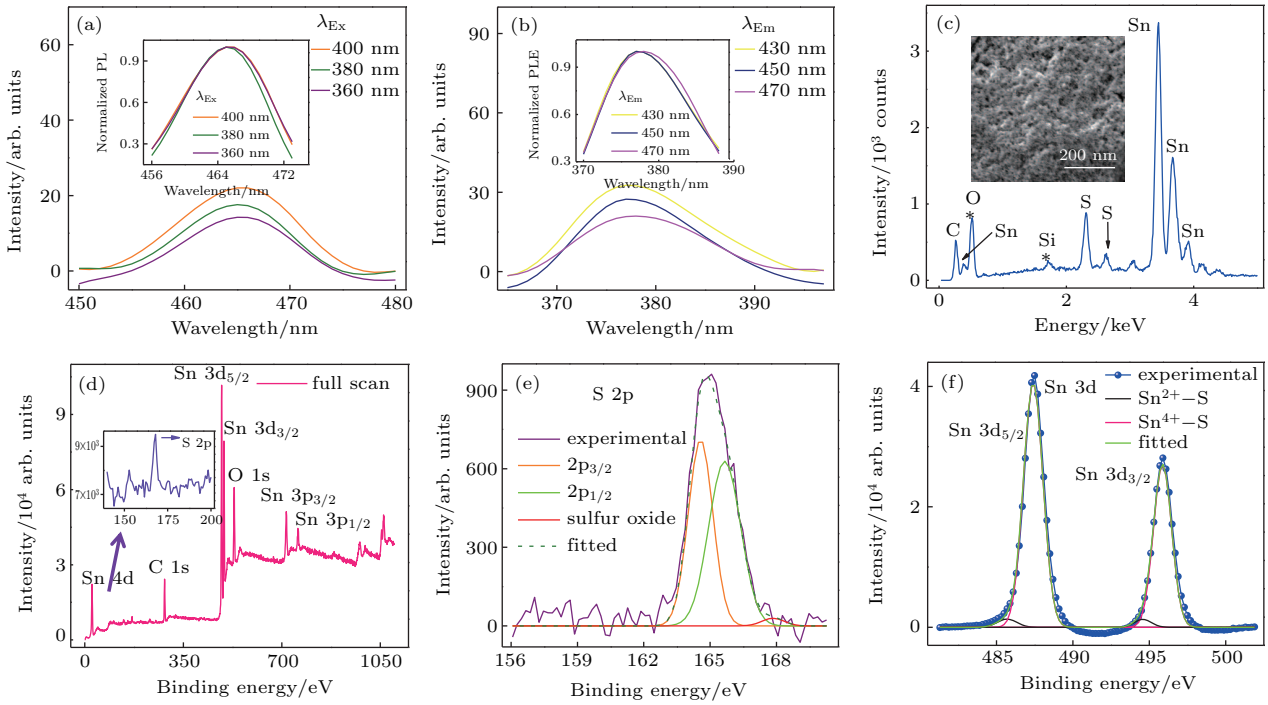


Fig. 2. (a) The PL spectra of SnS_2 QDs aqueous solution excited by various wavelengths and corresponding normalized PL spectra of the SnS_2 QDs. (b) The PLE spectra of SnS_2 QDs aqueous solution and normalized PLE spectra of the SnS_2 QDs. (c) EDS spectrum and SEM image of the SnS_2 QDs on a Si substrate (inset: SEM image). (d) The full-scan XPS spectrum of SnS_2 QDs. (e) The XPS S 2p spectrum of the SnS_2 QDs. (f) The XPS Sn 3d spectrum of the SnS_2 QDs.

3.2. Characterization of devices

The fabrication processes of the SnS_2-QDs-based photodetectors consisting of interdigital gold electrodes are shown in Fig. 3(a). The SnS_2 QDs solution was drop-casted onto the interdigitated electrodes and dried at 50 °C on a heating plate in the air. The as-prepared interdigitated electrodes can be

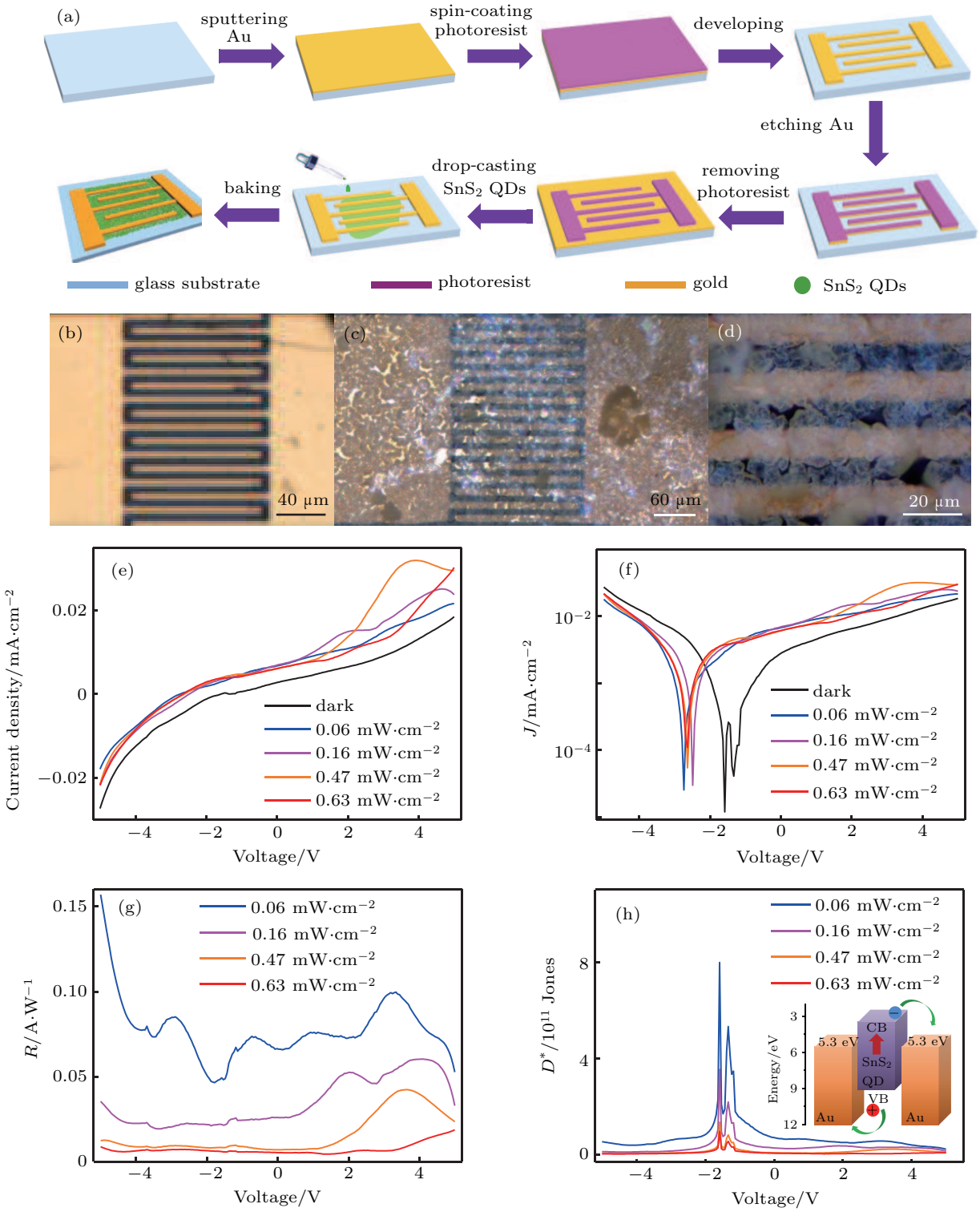


Fig. 3. (a) Schematic diagrams illustrating the fabrication process of the SnS_2 QDs photodetector. (b) The prepared interdigitated gold electrodes. (c) The SnS_2 QDs solution was drop-casted onto the interdigitated electrodes. (d) The enlarged image of the interdigitated electrodes under the microscope. (e) The J–V curves of the detector in the dark and under illumination at 365 nm with different light intensities. (f) log(J)–V curves. (g) R–V curves. (h) D^*–V curves (inset: the energy band diagram of the detector).

observed using an optical microscope as shown in Fig. 3(b). Interdigitated electrodes covered with SnS_2 QDs can be observed at different magnifications in Figs. 3(c) and 3(d), which show homogeneous and yellow QDs films. The J–V curve of the UV detector irradiated by $\lambda = 365$ nm light under the conditions of 0 mW·cm^{-2}, 0.06 mW·cm^{-2}, 0.16 mW·cm^{-2}, 0.47 mW·cm^{-2}, and 0.63 mW·cm^{-2} is shown in Fig. 3(e). The current density increases under light irradiation, suggesting that the device responds to light and exhibits good photoelectric performance. Figure 3(f) shows the log(J)–V curve, from which it can be seen that the light current of the device is larger than the dark current. Therefore, the device is suitable

for use in ultraviolet detection.

We discuss the responsivity R and detectivity D^* of the photodetector using the following expression:[28]

$$R = J_{\rm ph}/P_{\rm opt}, \tag{4}$$

$$D^* = \frac{R}{\sqrt{2q/J_{\rm d}}}, \tag{5}$$

where $J_{\rm ph}$ is the photocurrent density, $P_{\rm opt}$ is the photo power density, q is the absolute electron charge (1.6×10^{-19} coulombs), and $J_{\rm d}$ is the dark current density. The value of R is relatively small in Fig. 3(g), however, the response rate increases as the reverse bias voltage increases. The D^* stabilizes at 10^{11} Jones (1 Jones = 1 cm·Hz$^{1/2}$·W^{-1}) and the detection rate increases as the light intensity decreases, indicating that the device is suitable for detecting light intensity. The energy band diagram of the detector is shown in the inset of Fig. 3(h). When ultraviolet light irradiates on the device, SnS_2 QDs absorb ultraviolet photons, and electrons are excited from the valence band (VB) to the conduction band (CB), forming photogenerated electrons and photogenerated holes (excitons). Under the bias electric field, excitons are dissociated and collected by the electrodes, which is the UV photoelectric detection mechanism of SnS_2 QDs.

Resistance–temperature (R–T) characteristic of the detector based on SnS_2 QDs is shown in Fig. 4(a). The resistance is about 10^6 Ω, and it is obvious that the resistance increases linearly with the increase of the temperature. The resistivity ρ of the device is also calculated according to the electrode structure at different temperatures in order to understand the electrical properties of the QDs detector. The resistivity of the detector at different temperatures is calculated using the following formula:

$$\rho = R\frac{(N-1)\,\omega d}{l}, \tag{6}$$

where R is the resistance, N is the number of interdigitated electrodes, ω is the overlap length of interdigitated electrodes, l is the spacing between the interdigitated electrodes, and d is the film thickness. The ρ–T curve of the detector is shown in Fig. 4(b).

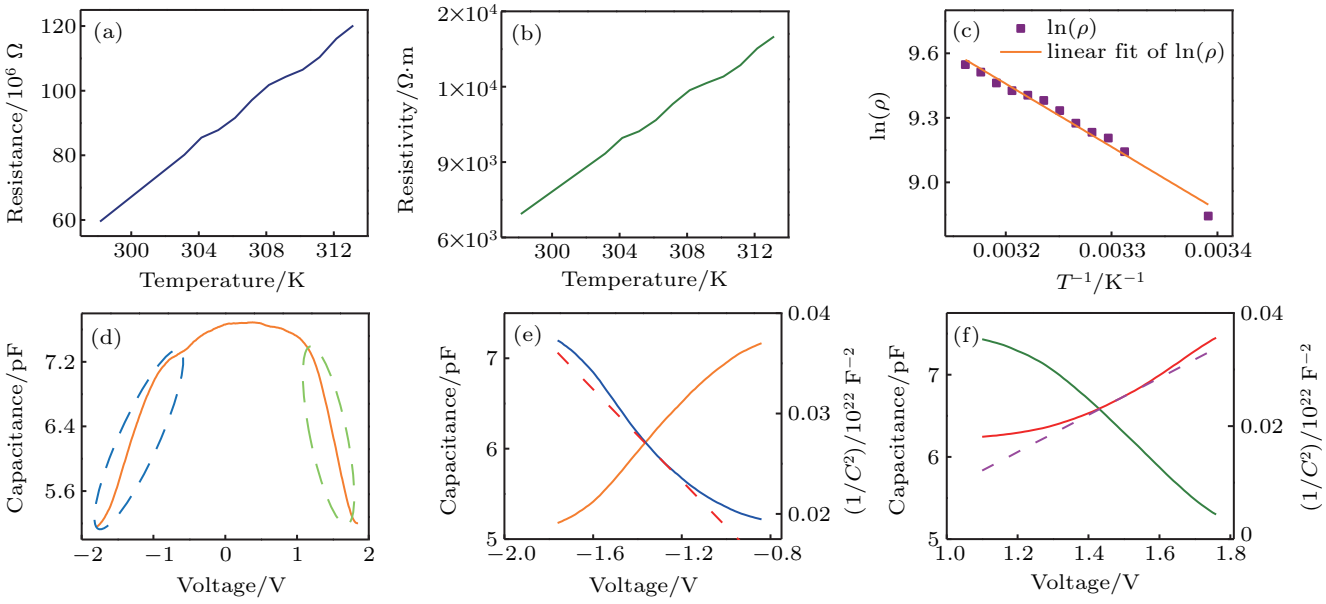


Fig. 4. (a) The R–T curve of the detector based on SnS_2 QDs. (b) The ρ–T curve of the detector based on SnS_2 QDs. (c) The $\ln(\rho)$–$1/T$ curve of the detector based on SnS_2 QDs. (d) The C–V curves of the SnS_2 QDs detector. (e) The C–V curves and plots of $1/C^2$ vs. V for the detector which is divided into two parts, corresponding to (e) and (f), respectively.

In general, the resistivity of a semiconductor decreases as the temperature increases. However, the observed resistivity of the SnS_2 QDs based detector is different from the conventional semiconductors. For semiconductors with impurity, the resistivity increases with temperature near room temperature[29] and the SnS_2 QDs based detector shows similar property in this aspect. In the above EDS and XPS spectra, it is evident that oxygen is present in the SnS_2 QDs and oxygen could act as impurity, hence the SnS_2 QDs based detector exhibits a behavior similar to the semiconductors with impurity. The $\ln(\rho)$–$1/T$ curve shown in Fig. 4(c) can be explained using the following expressions:

$$\rho = E\exp\left(E_{\rm a}/k_{\rm B}T\right), \tag{7}$$

where E is a pre-exponential factor, $E_{\rm a}$ is the thermal activation energy, $k_{\rm B}$ is the Boltzmann constant, and T is the absolute temperature. Take natural logarithm on both sides of Eq. (7)

$$\ln(\rho) = \ln(A) + E_{\rm a}/\left(k_{\rm B}\cdot T\right). \tag{8}$$

The unary linear regression of the values $\ln(\rho)$–$1/T$ is carried out in Eq. (7), which is shown in Fig. 4(c). The thermal activation energy and index factor of the detector can be calculated

with the obtained intercept and slope, respectively. Table 1 shows the respective data and calculated values. The regression coefficient in Table 1 is 0.98, which is very close to 1, indicating that $\ln(\rho)$ and $1/T$ have a good linear relationship and the large pre-exponential factor results in a large resistivity of the device.

Table 1. Relative parameters of the device, the calculated value of the thermal activation energy, and the index factor.

Intercept $\ln(E)/\Omega\cdot$m	Slope $\lvert E_a/k_B\rvert$	Regression coefficient	$E/\Omega\cdot$m	$\lvert E_a\rvert$/eV
22.96	4.19×10^3	0.98	9.33×10^9	0.36

The C–V plots and the variation of $1/C^2$ at room temperature under 1 kHz illumination at voltage range from -2 V to 2 V are shown in Fig. 4(d). Under a bias, the C–V relationship can be expressed as[30]

$$C^{-2} = \frac{2(V_{bi} - V)}{q\varepsilon_0\varepsilon_r N F^2}, \tag{9}$$

where V_{bi} is the built-in potential at zero bias, ε is the permittivity of a vacuum, ε_r is the relative permittivity of the material, N is the carrier concentration in the depletion layer, and F is the photosensitive area (3.33×10^{-4} cm^2). The x-intercept is V_{bi}, and N can be calculated from the slope of the linear part of the curve between $1/C^2$ and V

$$N = \frac{-2}{q\varepsilon_0\varepsilon_r F^2}\left[\frac{\partial\left(C^{-2}\right)}{\partial V}\right]^{-1}, \tag{10}$$

where ε_r for SnS_2 QDs is 20.[15]

The depletion layer width W_d is expressed as

$$W_d = \left[\frac{2\varepsilon_0\varepsilon_r\left(V_{bi} - V\right)}{qN}\right]^{1/2}. \tag{11}$$

The change in capacitance on the left and right parts of the curve in Fig. 4(d), which are circled in different colors, have been analyzed in Figs. 4(e) and 4(f), respectively. Table 2 shows the data obtained. As the structure of Au/SnS_2 QDs/Au devices has no polarity, the C–V curve is symmetrical. The values of V_{bi}, N, and W_d are similar under positive and negative biases. Compared to other photodetectors,[31] the values of V_{bi}, N, and W_d of the detector based on SnS_2 QDs are similar to graphene QDs based photovoltaic detector. Graphene based heterojunctions have been widely studied,[32–34] and it is found that different heterojunctions formed by different materials or different conductive types (n-type or p-type) materials result in different C–V curve characteristics. For asymmetric unipolar heterojunctions, C–V curves are mostly monotonous, while for non-polar symmetrical heterojunctions, C–V curves are symmetric with $V = 0$ V. Apparently, our Au/ SnS_2 QDs/Au device belongs to the latter case (symmetric C–V curve).

Table 2. The built-in potential, carrier concentration and depletion layer width of SnS_2 QDs heterojunction at 1 kHz.

SnS_2 QDs	V_{bi}/V	$N/10^{18}$ cm^{-3}	W_d/nm ($V = 0$)
Negative bias	0.95	1.36	15.44
Positive bias	0.74	1.43	11.44

4. Conclusion

In conclusion, homogeneous and monodispersed SnS_2 QDs have been synthesized for the first time using a low-cost, facile, green, and effective method under ambient pressure and a temperature lower than 80 °C. The size and morphology of the SnS_2 QDs have been characterized using TEM and AFM techniques. SnS_2 QDs have small dimension with an average particle size of 4.2 nm and they exhibit good crystallinity. The absorption of the SnS_2 QDs solution is observed in the ultraviolet band. The performance of the photodetector based on SnS_2 QDs is stable as the J–V curve remains unchanged during repeated measurements. Under $\lambda = 365$ nm illumination, the response rate R of the photodetector is greater than 0.10 A·W^{-1}, and the detection rate D^* is about 10^{11} Jones. This work demonstrates the use of the SnS_2 QDs prepared using the facile method in UV photodetector, which shows excellent performance.

References

[1] Lee M J, Ahn J H, Sung J H, Heo H, Jeon S G, Lee W, Song J Y, Hong K H, Choi B, Lee S H and Jo M H 2016 *Nat. Commum.* **7** 12011
[2] Buscema M, Barkelid M, Zwiller V, van der Zant H S J, Steele G A and Gomez A C 2013 *Nano Lett.* **13** 358
[3] Li X, He D W, Wang Y S, Hu Y, Zhao X, Fu C and Wu J Y 2018 *Chin. Phys. B* **27** 056104
[4] Xia J, Zhu D D, Wang L, Huang B, Huang X and Meng X M 2015 *Adv. Funct. Mater.* **25** 4255
[5] Zhou X, Gan L, Zhang Q, Xiong X, Li H Q, Zhong Z Q, Han J B and Zhai T Y 2016 *J. Mater. Chem. C* **4** 2111
[6] Zhou X, Zhang Q, Gan L, Li H Q and Zhai T Y 2016 *Adv. Funct. Mater.* **26** 4405
[7] Ou J Z, Ge W Y, Carey B, Daenake T, Rotbart A, Shan W, Wang Y C, Fu Z Q, Chrimes A F, Wlodarski W, Russo S P, Li Y X and Kalantar-zadeh K 2015 *ACS Nano* **9** 10313
[8] Seo J, Jang J, Park S, Kim C, Park B and Cheon J 2008 *Adv. Mater.* **20** 4269
[9] Klimov V I, Mikhailovsky A A, Xu Su, Malko A, Hollingsworth J A, Leatherdale C A, Eisler H J and Bawendi M G 2000 *Science* **290** 314
[10] Tang Jing and Xu X L 2018 *Chin. Phys. B* **27** 027804
[11] Gao L, Chen C, Zeng K, Ge C, Yang D, Song H S and Tang J 2016 *Light: Sci. & Appl.* **5** e16126
[12] Yuan Y J, Chen D Q, Shi X F, Tu J R, Hu B, Yang L X, Yu Z T and Zou Z G 2017 *Chem. Eng. J.* **313** 1438
[13] Tan F R, Qu S C, Wu J, Liu K, Zhou S Y and Wang Z G 2011 *Nanoscale Res. Lett.* **6** 298
[14] Qiao B, Zhao S L, Xu Z and Xu X R 2016 *Chin. Phys. B* **25** 098102
[15] Fu X, Ilanchezhiyan P, Kumar G M, Cho H D, Zhang L, Chan A S, Lee D J, Panin G N and Kang T W 2017 *Nanoscale* **9** 1820
[16] Truong N T N and Park C 2016 *Electron. Mater. Lett.* **12** 308
[17] Tsukigase H, Suzuki Y, Berger M H, Sagawa T and Yoshikawa S 2011 *J. Nanosci. Nanotechnol.* **11** 3215
[18] Yin Y and Alivisatos A P 2005 *Nature* **437** 664
[19] Zhai C X, Du N and Yang H Z D 2011 *Chem. Commun.* **47** 1270
[20] Tu J R, Shi X F, Lu H W, Yang N X and Yuan Y J 2016 *Mater. Lett.* **185** 303
[21] Bharatula L D, Erande M B, Mulla I S, Rout C S and Late D J 2016 *RSC Adv.* **6** 105421

[22] Tan F R, Qu S C, Zeng X B, Zhang C S, Shi M J, Wang Z J, Jin L, Bi Y, Cao J, Wang Z G, Hou Y B, Teng F and Feng Z H 2010 *Solid State Commun.* **150** 58

[23] Lin C X, Zhu M S Q, Zhang T, Liu Y F, Lv Y C, Li X J and Liu M H 2017 *RSC Adv.* **7** 12255

[24] Yuan H, Sutter E, Sadowski J T, Cotlet M, Monti O L A, Racke D A, Neupane M R, Wickramaratne D, Lake R K, Parkinson B A and Sutter P 2014 *ACS Nano* **8** 10743

[25] Satoh N, Nakashima T, Kamikura K and Yamamoto K 2008 *Nat. Nanotechnol.* **3** 106

[26] Li X L, Chu L B, Wang Y Y and Pan L S 2016 *Mat. Sci. Eng. B* **205** 46

[27] Ham G, Shin S, Park J, Lee J, Choi H, Lee S and Jeon H 2016 *RSC Adv.* **6** 54069

[28] Gong X, Tong M H, Xia Y J, Cai W Z, Moon J S, Cao Y, Yu G, Shieh C L, Nilsson B and Heeger A J 2009 *Science* **325** 1665

[29] Liu E K, Zhu B S and Luo J S 2011 *The Physics of Semiconductors* (7th edn.) (Beijing: Publishing House of Electrics Industry) p. 111 (in Chinese)

[30] Ramar M, Suman C K, Manimozhi R, Ahamad R and Srivastava 2014 *RSC Adv.* **4** 32651

[31] Zhao J H, Tang L B, Xiang J Z, Ji R B, Hu Y B, Yuan J, Zhao J, Tai Y J and Cai Y H 2015 *RSC Adv.* **5** 29222

[32] Miao X C, Tongay S, Petterson M K, Berke K, Rinzler A G, Appleton B R and Hebard A F 2012 *Nano Lett.* **12** 2745

[33] Shivareman S, Herman L H, Rana F, Park J and Spencer M G 2012 *Appl. Phys. Lett.* **100** 183112

[34] Singh A, Uddin M A, Sudarshan T and Koley G 2014 *Small* **10** 1555